

The use of Computational Fluid Dynamics to Determine the Dynamic Stability of an Autonomous Underwater Vehicle

Alexander Phillips*, Maaten Furlong** and Stephen R Turnock*

*Fluid-Structure Interaction Research Group, School of Engineering Sciences, University of Southampton, Highfield, Southampton SO17 1BJ, UK

**National Oceanography Centre, Southampton, European Way, Southampton, SO14 3ZH, UK

Corresponding author's email: abp@soton.ac.uk

Introduction

Various forms of Autonomous Underwater Vehicles (AUVs) have evolved to solve different subsea mission requirements, these can be loosely grouped into two types: torpedo style AUVs and hovering AUVs. Torpedo AUVs were initially developed to be launched from torpedo tubes and consequently resemble torpedoes with a propeller and control surfaces at the rear, these vehicles have poor slow speed maneuverability due to inefficiency of the control surfaces at low speed, but have good straight line performance due to their streamlined shape. AUVs of this type are predominantly used for pipeline inspection, environmental monitoring, scientific research and other long range applications.

Hovering AUVs tend to be used for applications where a greater level of slow speed maneuverability is required. These vehicle use a number of thrusters to maintain depth and heading control.

The eventual aim of the program of work under way is to develop specific AUV hull concept design techniques that are robust and reliable. To this end, Computational Fluid Dynamics (CFD) analysis methods are being investigated which combine automated meshing and parametric hull shape definitions to reduce overheads when evaluating the design of a concept AUV hull. Since each AUV application requires varying levels of dynamic stability and maneuverability this work uses steady state CFD analysis to determine numerically the dynamic stability of an AUV. In order to verify the methodology the procedure has been performed for the torpedo style AUV Autosub, (see Fig 1), for which there is suitable experimental data to benchmark the solutions.



Figure 1: Autosub

Autosub is a large AUV developed by a team of engineers and oceanographers at the National Oceanography Centre, Southampton. Autosub's principle dimensions are listed below:

- Length 7 m
- Diameter 0.9 m
- Speed Range 1.0 - 2.0 m/s
- Operating Reynolds Number (RN) 5.9×10^6 - 11.8×10^6

Autosub is controlled by four movable control surfaces mounted at the rear of the vessel in a cruciform arrangement. Two vertical rudders control the yaw of the vessel, while two horizontal stern planes adjust the pitch of the vessel. Autosub has been employed in scientific research projects ranging from mapping manganese distributions in a sea loch to under ice exploration in the Arctic and Antarctic [10] [11]. Autosub's missions predominantly comprise of long range transit missions where good dynamic stability is an advantage.

The dynamic stability of an AUV determines the how the vehicle behaves when disturbed while initially travelling on a straight course with no control plane input.

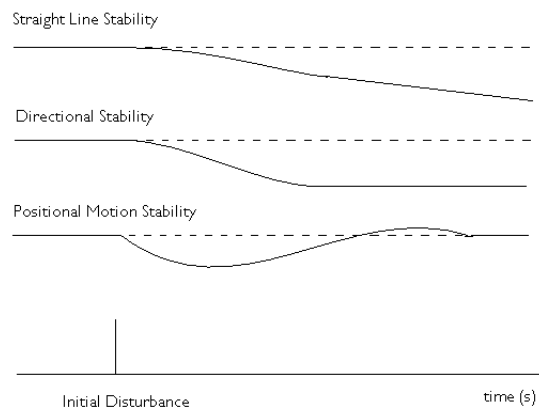


Figure 2: Dynamic Stability

The levels of motion stability are detailed in Figure 2 which illustrates the response of a vehicle to an initial disturbance:-

- Straight line stability - the final course some time after the disturbance is straight, but heading is not maintained.
- Directional stability - the final course is straight on the same heading, but with a different position.
- Positional stability - The final path is the same as the initial path.

With zero control input the linearised equations of motion of a submerged vehicle in the horizontal plane reduce to [1]: -

$$(m - Y_{\dot{v}})\dot{v} = Y_v v + (Y_r - mV)r \quad (1)$$

$$(I_{zz} - N_{\dot{r}})\dot{r} = N_v v + Y_r r \quad (2)$$

The surge and sway velocities u and v are the velocity components of the origin placed at amidships, where V is the initial velocity of the vessel. The yaw rate r is the angular velocity about the vertical axis. X represents the surge force, Y the sway force and N the yaw moment. The derivative notation $Y_v = \frac{\partial Y}{\partial v}$ is used.

By applying the Routh stability criteria the determinant of dynamic stability in sway and yaw is:-

$$N_r Y_v - N_v (Y_r - mV) > 0 \quad (3)$$

Dividing through by Y_v and $(Y_r - mV)$ results in

$$\frac{N_r}{(Y_r - mV)} - \frac{N_v}{Y_v} > 0 \quad (4)$$

The first term represents the ratio of the moment caused by yaw rotation divided by the force due to the rotation, hence equates to the point of action of the force due to the yaw motion \bar{x}_r . Similarly the second term equates to the point of action of the force due to the sway motion \bar{x}_y . Hence the criteria for dynamic stability in the horizontal plane is $\bar{x}_r - \bar{x}_y > 0$ For a more detailed discussion see [1].

Rewriting Equation 4 as the horizontal stability margin G_H :-

$$G_H = 1 - \frac{N_v(Y_r - mV)}{N_r Y_v} \quad (5)$$

A stability margin of less than 1 represents a dynamically stable vehicle. The calculations are similar in the vertical plane. Since Autosub is axisymmetric in the xz and xy planes the stability margin in the vertical plane, G_V , will have the same value as G_H at higher speeds.

Hydrodynamic derivatives N_r , N_v , Y_r and Y_v are traditionally derived from model tests [6] [4] or empirical formulations [8], but have also been derived numerically from inviscid flow methods or from observations[5].

Either steady state experiments using a combination of steady state, drift tests and rotating arm experiments or unsteady Planar Motion Mechanism (PMM) tests can be used. For this study the steady state experiments are replicated numerically.

Yawed drift angle tests in a towing tank tests induce a sway velocity (v) component and the corresponding sway force (Y) and yaw moment(N) acting on the model can be deduced and plotted from which the rate coefficients Y_v and N_v may be determined from the gradient of the graph.

Rotating arms are used to measure the rotary derivatives of a vessel, by imposing an angular velocity on a vessel by attaching it to the end of a rotating arm. The centre line of the vessel is aligned with the tangent of the circle while the transverse direction is orientated with the arm.

The model is rotated at constant linear speed (u) at various radii (R) thus varying the angular velocity (r) while the dynamometer measures the sway force (Y) and yaw moment (N). These results are plotted and the values Y_r and N_r may be determined from the gradient of the plot.

Experimental rotating arm experiments have several limitations: -

- rotating arm experiments require large specialised and expensive facilities. In order to determine the values of Y_r and N_r as $r \rightarrow 0$ the radius (R) should be large in relation to the vehicle length (L).
- the model must be accelerated and tests performed within a single revolution to ensure the vessel is not disturbed by its own wash, this limits the duration of each run.

By performing virtual tests in a numerical towing tank these limitations can be overcome.

Model scale tests were performed on a nearly $2/3^{rd}$ scale model of the Autosub hull form by Kimber et al. [6] at the HASLAR facility (270 m \times 12.2 m \times 5.5 m deep). Steady state experiments were performed at drift angles of $\pm 0^\circ$, $\pm 2^\circ$, $\pm 4^\circ$, $\pm 6^\circ$, $\pm 8^\circ$ and $\pm 10^\circ$ with a rudder angle of 0° . Rotating arm experiments were performed at radius of 13, 17.358 and 26m all at a circumferential velocity of 2.69m/s.

Method

The fluid flow around Autosub has been modelled using the commercial finite volume code ANSYS CFX 11 (CFX) [3]. For these calculations the fluid's motion is modelled using the incompressible (6), isothermal Reynolds Averaged Navier Stokes (RANS) equations (7) in order to determine the cartesian flow field ($u_i = u, v, w$) and pressure (p) of the water around an AUV hull:

$$\frac{\partial \bar{U}_i}{\partial x_1} = 0 \quad (6)$$

$$\frac{\partial \bar{U}_i}{\partial t} + \frac{\partial \bar{U}_i \bar{U}_j}{\partial x_j} = -\frac{1}{\rho} \frac{\partial P}{\partial x_i} + \frac{\partial}{\partial x_j} \left\{ \nu \left(\frac{\partial \bar{U}_i}{\partial x_j} + \frac{\partial \bar{U}_j}{\partial x_i} \right) \right\} - \frac{\partial \overline{u'_i u'_j}}{\partial x_j} + f_i \quad (7)$$

By time averaging the Navier Stokes equations to generate the RANS equations, 6 further unknowns have been created, termed the Reynolds stresses:

$\frac{\partial \overline{u'_i u'_j}}{\partial x_j}$. Various turbulence models are used to provide solutions to the Reynolds stresses in terms of known quantities to allow closure of the RANS equations [12]. Different turbulence models have been tailored to different types of turbulent flows. The $k - \epsilon$ model is a commonly used turbulence model for engineering simulations due to its robustness and application to a wide range of flows. However it is known to be poor at locating the onset and extent of separation [2]. As an alternative the Shear Stress Transport (SST) model is better at predicting separation [2] likely to be found at the aft end of the AUV.

To determine the relative performance of these two turbulence models both the $k - \epsilon$ and SST model have been used for this study.

The rapid production of high quality grids for a parametric series of AUV orientations is desirable if consistent set of quality meshes are to be produced. For this study, the meshes are produced by careful parameterisation of the AUV hull using Tool Command Language (TCL) script files for driving the meshing package ANSYS ICEM CFD.

Numerical Drift Tests

For the steady state drift tests the scripts produce high quality multi-block structured grids with detailed control over the essential mesh parameters. The fluid domain is defined as a cuboid fixed in space. An inlet boundary condition is positioned 0.5 bodylengths upstream with an inflow velocity of 2.69m/s and a inflow turbulence of 5%. An outlet boundary condition with zero relative pressure is defined 3 body lengths downstream. Free slip wall boundary conditions are applied to the 4 remaining walls which are 3 diameters from the AUV and a no slip boundary condition is applied to the hull, see figure 3.

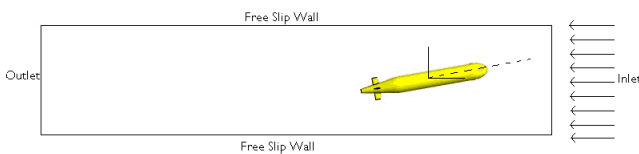


Figure 3: Boundary Conditions for the Numerical Drift Tests

The far field is modelled using a H topology with a O grid topology wrapped around the AUV to give control over the boundary layer parameters. Prior to running simulations the mesh parameters required to adequately model the boundary layer were estimated using the following equations proposed by CFX [3].

The first layer thickness for a desired y^+ can be estimated from: -

$$\Delta y = L \Delta y^+ \sqrt{80} R_n^{-13/14} \quad (8)$$

The boundary layer for a blunt body can be estimated using the following equation: -

$$\delta = 0.035 L R_n^{-1/7} \quad (9)$$

From these equations a first cell thickness of 1mm was selected this results in a $20 \leq \Delta y^+ \leq 200$ with a total of 15 elements within the boundary layer.

Numerical Rotating Arm Experiments

For comparison purposes the rotating arm tests the scripts produce unstructured tetrahedral meshes with inflated prism layers surrounding the AUV.

To replicate the rotary motion the domain is defined as a rotating domain with its origin at the fixed end of the rotating arm. The fluid modelled comprises a segment of a ring with a rectangular cross section, see figure 4.

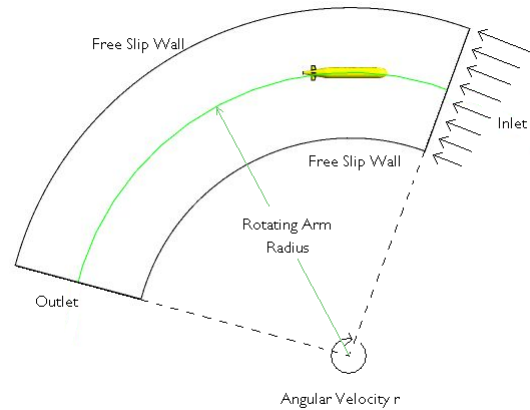


Figure 4: Boundary Conditions for the Numerical Rotating Arm Experiments

For each rotating arm radius the angular velocity is modified to give a velocity of 2.69m/s along the centreline of the AUV.

Computer Simulation

Simulations were run on a high specification desktop pc running 64 bit Windows XP with 4 GB of RAM. Solutions presented have been calculated using the high resolution advection scheme. The residual mass error was reduced by four orders of magnitude and lift and drag forces on the AUV were monitored to ensure convergence. Typical run times took two wall clock hours.

Results

The results are non-dimensionalised by the length of the vehicle (L) the velocity of the vehicle (V) and the density of the fluid (ρ), a prime symbol is used to signify the non dimensional form for example:

$$v' = \frac{v}{V} \quad (10)$$

$$Y' = \frac{Y}{1/2\rho L^2 V^2} \quad (11)$$

$$N' = \frac{N}{1/2\rho L^3 V^2} \quad (12)$$

Drift Tests

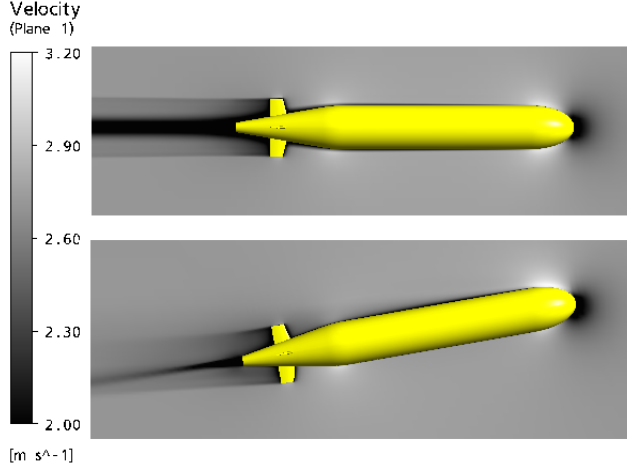


Figure 5: Velocity profile about Autosub at 0° (top) and 10° (bottom) incidence

Figure 5 compares demonstrates the variation in fluid velocity around the hull at an angle of incidence of 0° and 10°, this equates to a sway velocity of 0m/s and 0.47m/s respectively. Plots of X' versus sway velocity (v'), Y' versus sway velocity (v'), N' versus sway velocity (v') are presented in Figures 6, 7 and 8.

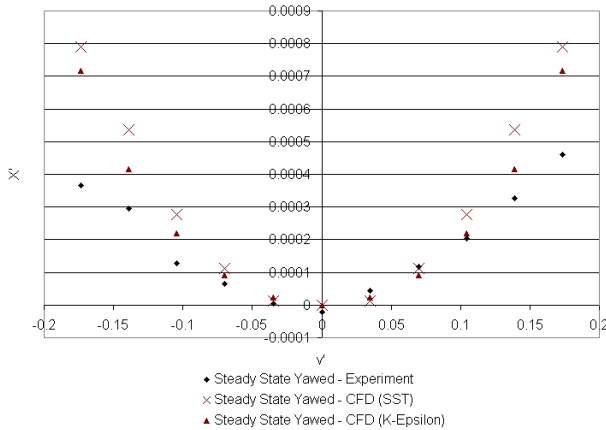


Figure 6: Drift Test - Variation of Surge Force with Sway Velocity

Rotating Arm

Figure 9 illustrates the fluid velocity around Autosub in a rotating domain with a radius of 17.328m. Plots of Y' versus yaw velocity (r') and N' versus yaw velocity (r') are presented in Figures 10 and 11.

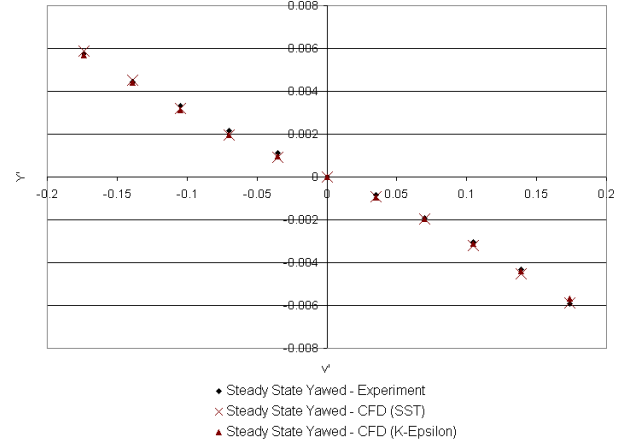


Figure 7: Drift Test - Variation of Sway Force with Sway Velocity

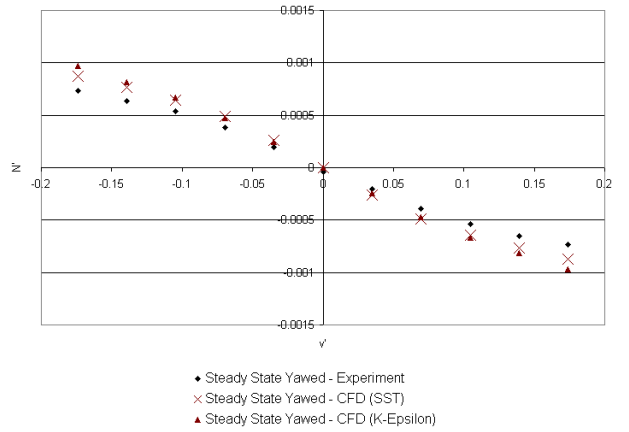


Figure 8: Drift Test - Variation of Yaw moment(N) with Sway Velocity (v)

Dynamic Stability

Table 1 compares the numerical and experimental values for the hydrodynamic derivatives derived from gradients of the previous plots.

Entering the results from table 1 into equation 5 gives an experimental stability margin of $G_H = 0.75$ compared with values of 0.72 and 0.73 determined numerically using $k - \epsilon$ and SST models respectively.

Discussion

Two separate automated meshing strategies were used in the creation of the mesh for the yawed drift and rotating arm tests. The structured meshing strategy used for the drift tests required significant time at the start of the study to automate the blocking procedure to allow for various body orientations, however once defined creation of a new mesh takes less than 5 minutes. The unstructured meshes used for the rotating arm experiments required a much lower initial

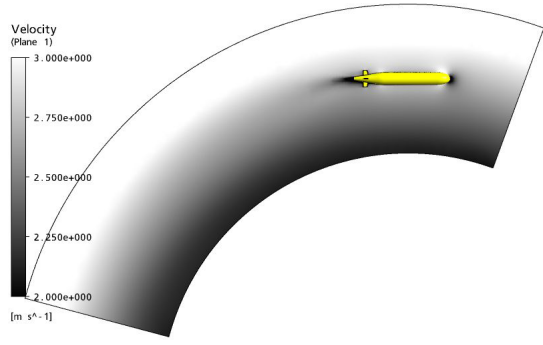


Figure 9: Velocity Profile - Rotating Arm Radius 17.328m

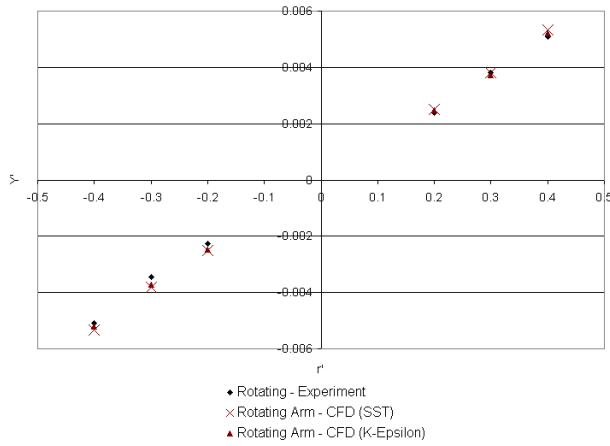


Figure 10: Rotating Arm - Variation of Sway Force with Yaw Velocity

time investment but take approximately 20 minutes to generate a smoothed mesh. Both mesh strategies produced good quality meshes, which gave good results however for study's of this nature where multiple meshes are required the use of structured mesh with a constant mesh topology results in less uncertainty due to variation in the mesh.

For both sets of experiments, the sway force (Y') is very well captured by the numerical experiments with negligible variation between the $k - \epsilon$ and SST turbulence models, for the drift case the predicted values lie within the experimental uncertainty associated with \pm yaw angles.

The trends in yaw moment (N') variation with angle of incidence are well predicted by the SST model, which correctly predicts the reduction in the gradient $\frac{\partial Y'}{\partial v'}$ at higher sway velocities. Both turbulence models over predict the magnitude of the yaw moment by approximately 20%.

The induced drag is also over predicted by the CFD simulations.

The numerical predictions of Autosub's dynamic

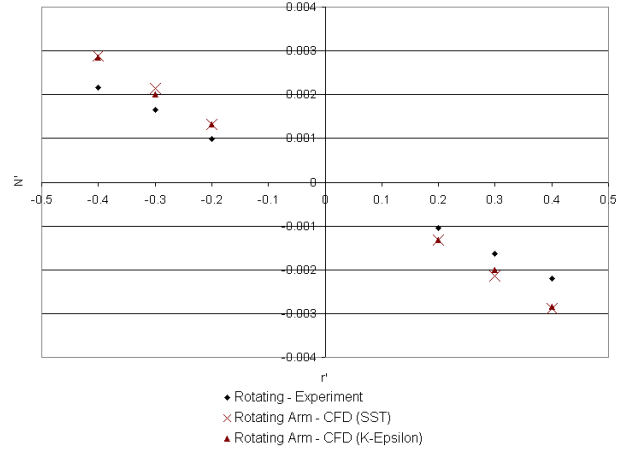


Figure 11: Rotating Arm - Variation of Yaw moment(N) with Yaw Velocity (v)

Table 1: Comparison of Experimental and CFD Values for the Hydrodynamic Derivatives all values are non-dimensional and x1000

Derivative	Experimental	CFD (K-epsilon)	CFD (SST)
Y'_v	-28.45	-27.28	-26.57
N'_v	-4.5	-5.90	-5.50
Y'_r	12.64	12.35	12.50
N'_r	-5.35	-6.59	-6.64

stability margin are good.

It is believed that the discrepancies in the experimental and numerical predictions of the yaw moments and induced drag lies in the influence of hull and tip vortices on the flow. The AUV's rudders experiencing three-dimensional flow has very different characteristics than a foil experiencing two-dimensional flow. The flow will tend to spill over the rudder ends from the positive pressure side to the negative pressure side resulting in a tip vortex. Such a flow removes the pressure difference at the tips of the foil and decreases it over the entire span of the rudder. If insufficient elements are correctly positioned to correctly capture the radius of the vortex core, then the low pressure within the vortex will be poorly predicted [7].

Insufficient elements to resolve the vortex core results in diffused vortices which rapidly decay as seen in figure 12.

Capturing the vortex core requires a much finer mesh than the surrounding potential flow. Increasing the mesh density of the entire fluid domain is impractical. The use of courser meshes with finer elements clustered in the vicinity of the vortices is more practical but requires knowledge of the vortex location prior to simulation or the use of adaptive meshing techniques to move the mesh [9].

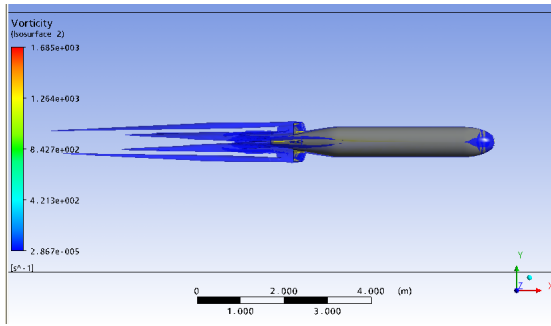


Figure 12: Vortex Structure around Autosub at 10° Incidence

Conclusions

Steady state CFD has been used to successfully replicate yawed towing tank and rotating arm experiments for a torpedo style AUV to derive the steady state hydrodynamic derivatives. Very good agreement was found for the prediction of sway forces, while the induced drag and yaw moments were marginally over predicted.

The dynamic stability margin of Autosub was well predicted by the numerical methods giving close agreement with the experimental value.

Further work

This work forms part of a study to produce a full unsteady hydrodynamic model of the AUV Autosub. Work is ongoing to integrate vortex capture techniques to better predict the influence of tip vortices on the flow to enable better prediction of the forces and moments acting on an AUV.

Acknowledgements

Mr Phillips' PhD studentship is jointly financed by the School of Engineering Science and the National Oceanography Centre, Southampton.

References

- [1] Roy Burcher and Louis Rydill. *Concepts in Submarine Design*. Cambridge University Press, 1994.
- [2] CFX. Innovative turbulence modeling: Sst model in ansys cfx. Technical report, ANSYS Ltd, 2006.
- [3] ANSYS CFX. *ANSYS CFX, Release 11.0*. ANSYS Ltd, 2007.
- [4] Jenhwa. Guo and Forng-Chen Chiu. Maneuverability of a flat-streamlined underwater vehicle. In *Proceedings of the 2001 IEEE International Conference on Robotics and Automation*. IEEE, 2001.
- [5] Joonyoung Kim, Kihun Kim, Hans S Choi, Woojae Seong, and Kyu-Yeul Lee. Estimation of hydrodynamic coefficients for an auv using nonlinear observers. *Journal of Oceanic Engineering*, 27(4), 2002.
- [6] N. Kimber and W. Marshfield. Design and testing of control surfaces for the autosub demonstrator test vehicle. Technical report, DRA Haslar, 1993.

- [7] Christos Pashias. *Propeller Tip Vortex Simulation Using Adaptive Grid Refinement Based On Flow Feature Identification*. PhD thesis, University of Southampton, 2005.
- [8] D. E. Perrault, T. Curtis, N. Bose, S. O'Young, and C Williams. C-scout manoeuvrability - a study in sensitivity. In *Oceans 01*. IEEE, 2001.
- [9] Pemberton Rj, Turnock Sr, Dodd Tj, and Rogers E. A novel method for identifying vortical structures. *Journal of Fluids and Structures*, 2002.
- [10] P.J. Statham, D.P. Connelly, C.R. German, T. Brand, J.O. Overnell, E. Bulukin, N. Millard, S. McPhail, M. Pebody, J. Perrett, Squire. M, P. Stevenson, and A. Webb. Spatially complex distribution of dissolved manganese in a fjord as revealed by high-resolution in situ sensing using the autonomous underwater vehicle autosub. *Environmental Science and Technology*, 2005.
- [11] P. Wadhams, J.P. Wilkinson, and S.D. McPhail. A new view of the underside of arctic sea ice. *Geophysical Research Letters*, 2006.
- [12] D. C. Wilcox. *Turbulence Modeling for CFD*. La Canada, Calif. : DCW Industries, 1998.